Journal of Magnetism and Magnetic Materials 322 (2010) 3131–3136

Contents lists available at ScienceDirect

Journal of Magnetism and Magnetic Materials

journal homepage: www.elsevier.com/locate/jmmm

Magnetotransport and magnetoelastic effects in Co-doped $La_{0.7}Sr_{0.3}MnO_3$ nanocrystalline perovskites

Sh. Tabatabai Yazdi [a], N. Tajabor [a,*], D. Sanavi Khoshnoud [b]

[a] Department of Physics, Faculty of Sciences, Ferdowsi University of Mashhad, Mashhad, Iran
[b] Department of Physics, Faculty of Sciences, Semnan University, Semnan, Iran

ARTICLE INFO

Article history:
Received 5 April 2010
Received in revised form
19 May 2010
Available online 2 June 2010

Keywords:
Manganite
Magnetoresistance
Magnetostriction
Thermal expansion
Nanoparticles

ABSTRACT

$La_{0.7}Sr_{0.3}Mn_{1-x}Co_xO_3$ ($x=0$, 0.05, 0.1) nanoparticles, prepared by sol–gel method, were studied by means of X-ray diffraction, transmission electron microscopy, resistivity, magnetoresistance, thermal expansion and magnetostriction measurements. Results show that partial substitution of Mn by Co leads to a reduction in lattice parameters, enhancement of resistivity and room temperature magnetoresistance MR, decrease of metal-insulator transition temperature T_{MI} and T_C, an increase in thermal expansion coefficient, volume magnetostriction and anisotropic magnetostriction. The latter increases about one order of magnitude with 10% Co substitution. In comparison with Mn ions, the Co ions possess higher anisotropy energy, larger magnetostriction effect, smaller ionic size and spin state transitions with increase in temperature and magnetic field; this suggests that Co substitution leads to double-exchange interaction weakening, resulting in suppression of ferromagnetic long-range order and metallic state and increase of magnetic anisotropy. Furthermore, our samples have a relatively lower T_{MI} and T_C, higher resistivity and MR, compared with the reported values for similar compounds with larger particle sizes. This is attributed to the nanometric grain size and spin-polarized tunneling between neighboring grains.

1. Introduction

The Mn-based perovskite oxides $RE_{1-x}A_xMnO_3$, where RE is a trivalent rare-earth ion (La, Pr, Y, Nd, etc.) and A is a divalent alkaline earth (Ca, Sr, Ba, etc.), have been a renewed subject of numerous investigations in recent years. The interest in them is not only because they are interesting systems exhibiting structural, magnetic and electronic transitions [1,2] but also because of their potential technological applications in various sensors and magnetomechanical devices arising from colossal magnetoresistance (CMR) and giant volume magnetostriction (GVMS) observed in certain compounds near room temperature [3–9]. Among a number of perovskite manganites with various combination of RE and A, $La_{1-x}Ca_xMnO_3$ and $La_{1-x}Sr_xMnO_3$ (LSMO) are prototypical and reference materials; however LSMO family has been studied much less.

The parent compound $LaMnO_3$ is an antiferromagnetic (AFM) insulator with $T_N \sim 140$ K; charge carriers are doped by substitution of La^{3+} with A^{2+} [1]. Although early theoretical considerations explained conductive and magnetic properties within the framework of Zener double-exchange (DE) interaction (transfer of the "extra" electron between neighboring Mn ions through the O^{2-} ions, resulting in an effective ferromagnetic interaction due to the strong on-site Hund's coupling [10,11]), more recent studies reveal the importance of Jahn–Teller distortion in the MnO_6 octahedra, in other words, formation of magnetic polarons in explaining the observed GMR values around T_c [11]. Localized electrons polarize the surrounding spins and result in ferromagnetic (FM) clusters. These microregions are referred to as ferrons, giant quasimolecules, magnetic polarons, etc. [12]. In compounds with high doping levels ($x \geq 0.17$ for A=Sr [3,7]), such FM regions grow and insulating AFM microregions are present in the conducting FM matrix. The cause of this magnetic two-phase state (MTPS) in manganites, which is confirmed experimentally by various methods including SEM and neutron scattering (e.g. [5]), is interpreted differently by different researchers, as a strong s–d exchange [5] and as a strong electron–phonon interaction.

Due to the close relation between transport, magnetotransport and magnetic properties of manganites, magnetostriction (MS) effects of these compounds have been attracting considerable attention since 1995. It has been found that a significant VMS effect around T_c is a common feature of all manganites [3–9,14] (it should be noted that the concept of T_C in MTPS is rather conditional, it is T_C of the FM part). So far, several mechanisms have been proposed for the MS effect in manganites, for example, Asamitsu et al. [1,2] attributed the observed GVMS in

* Corresponding author. Tel.: +98 511 8817741; fax: +98 511 8763647.
E-mail addresses: tajabor@ferdowsi.um.ac.ir, ntajabor@yahoo.com (N. Tajabor).

0304-8853/$ - see front matter © 2010 Elsevier B.V. All rights reserved.
doi:10.1016/j.jmmm.2010.05.046

$La_{0.83}Sr_{0.17}MnO_3$ single crystals to the structural transition caused by the applied magnetic field , or Koroleva et al. [3,7,12] explained the GVMS effect in $La_{0.7}Sr_{0.3}MnO_3$ single crystals on the basis of formation of small polarons and presence of FM/AFM two-phase state (MTPS) due to strong s–d exchange, etc. However, GVMS is not observed in conventional magnetic semiconductors with MTPS and CMR, since their lattices are rigid and the exchange s–d interaction is insufficient to overcome the electrostatic forces between ions [7].

The most attention to date has focused on doping the La sites in the parent compound, and far fewer studies have been conducted in doping the Mn sites. In this work, we have studied the effect of Mn substitution by Co on electrical, magnetotransport and magnetoelastic properties of $La_{0.7}Sr_{0.3}MnO_3$. In LSMO with $x=0.3$, $T_C\sim380$ K [15]; this promises well that the GVMS and CMR effects will take place in Co-doped LSMO around room temperature, appropriate for applications. Despite some previous research on Co-substituted LSMO studying their electrical, magnetic and magnetotransport properties [15–21], to date no report has been published on magnetoelastic properties of these compounds. So, in this work, we investigate the magnetostriction effects of $La_{0.7}Sr_{0.3}Mn_{1-x}Co_xO_3$ ($LSMC_xO$) along with their magnetotransport properties. It has been reported that Co reduces both T_C and MR [16], and composition with $x=0.1$ has the optimum conditions (showing a transition closer to room temperature with no harmful effects on magnetic and magnetotransport properties [22]).

2. Experiments

2.1. Synthesis

The $La_{0.7}Sr_{0.3}Mn_{1-x}Co_xO_3$ samples with $x=0$, 0.05 and 0.1 were prepared using a gel precursor in order to have well-mixed reagents. Stoichiometric amounts of $La(NO_3)_3\cdot6H_2O$, $Sr(NO_3)_2$, $Mn(NO_3)_2\cdot4H_2O$ and $Co(NO_3)_2\cdot6H_2O$ (MERCK, purity $>98\%$) were dissolved in distilled water under continuous stirring. Citric acid and ethylene glycol were added as complexation and polymerization agents, respectively, forming a stable solution (4 mol of citric acid and 3 mol of ethylene glycol for 1 mol of metal ions). This clear solution was then heated on a hot plate at temperatures ranging between 353 and 393 K, boiling off the excess solvent, and giving a yellowish gel. To remove the organic parts, the gel was further heated and dried at 473 K, resulting in foam, which was decomposed at 673 K in an oven, resulting in a porous precursor. After milling in an agate mortar, the precursor, in powder form, was calcinated at 873 K in air atmosphere for 10 h, and a second heat treatment with intermediate grinding was performed at 1073 K overnight before the final sintering. The black powder was cold pressed into pellets with diameter of 12 mm and thickness of about 3 mm under a pressure of 4 kbar and sintered at 1323 K for 24 h, resulting in hard black ceramic materials.

2.2. Characterization

Structural characterization of the nanocrystalline powders was carried out using X-ray powder diffraction (XRD) with monochromatic Cu Kα radiation ($\lambda\sim1.5406$ Å) in the 2θ range of 10–90° in a continuous scan mode with a step width of 0.05°. Analysis of the obtained profiles was performed using the Fullprof program, which is based on the Rietveld method. Sample morphology was studied using transmission electron microscopy (TEM) (LEO 912 AB, Carl Zeiss SMT, Germany, 120 kV). In this case, specimens were prepared from deposition of suspensions of powders in ethanol on copper grids coated with a carbon film. Electrical resistivity ρ and magnetoresistance $MR=(R_H-R_{H=0})/R_{H=0}$ measurements were performed by the standard four-probe technique on disk-shaped samples with a diameter of 10 mm and thickness of about 3 mm in the temperature range 80 — 320 K and fields up to 1.5 T. Their linear thermal expansion TE ($\Delta l/l=(l_T-l_{77\,K})/l_{77\,K}$) and magnetostriction (MS) were measured using the strain-gage technique on samples with a diameter of 6 mm and thickness of about 2 mm in the temperature range 80–430 K and magnetic fields up to 1.5 T. The accuracy of these measurements was better than 2×10^{-6}. The longitudinal ($\lambda_\parallel$) and transverse magnetostriction ($\lambda_\perp$) of samples were measured parallel and perpendicular to the applied magnetic field, respectively. The anisotropic MS (λ_t) and volume MS (ω) were calculated directly from the relations $\lambda_t=\lambda_\parallel-\lambda_\perp$ and $\omega=\lambda_\parallel+2\lambda_\perp$, respectively.

3. Results and discussion

The XRD patterns show that all samples are highly single phase with a small amount of La_2O_3 impurity (with an additional peak at around $2\theta=30^o$). In the case of $La_{0.76}Sr_{0.19}Mn_{1-x}Co_xO_3$ ($0\le x\le1$) synthesized by a conventional ceramic route with heat treatment at 1673 K, a similar kind of phase separation was also observed for compounds with $x\le0.2$ [20]. Reitveld analysis of patterns with the Fullprof program shows that the $LSMC_xO$ samples in the studied composition range crystallize in rhombohedral symmetry with space group R^-3c at room temperature, in agreement with the literature. Fig. 1 presents, as an example, the fitted diffraction pattern for the $LSMC_{0.05}O$ sample at 300 K. A satisfactory accordance of the observed and calculated diffraction patterns can be seen. The refined lattice parameters are summarized in Table 1. It is clear that although the structure does not undergo any change on partial replacement of Mn by Co, there is a slight reduction of lattice parameters and the cell volume as the co content increases. This is related to the small ionic radii of Co ion in different spin and valence states (Table 2).

The broadening of the XRD patterns peaks reveals the small particle (crystallite) size. The average particle size was calculated from the Scherrer's formula:

$$d=\frac{0.9\lambda}{\beta\cos\theta}$$

where $\lambda=1.5406$ Å, the X-ray wavelength, θ is the diffraction angle of a main reflection (0 2 4) and β is the full width at half maximum (FWHM) of that peak. In this way, the average particle size of about 18 nm is obtained.

The TEM photograph of $LSMC_{0.1}O$, as an example, is presented in Fig. 2. One can see polyhedral but nearly spherical nanoparticles posing an almost homogenous size distribution with the mean size of 20 nm, comparable with the value obtained from the broadening of XRD peaks. Though our sample is polydispersive, the particles have a reasonably narrow distribution, and the maximum particle size does not exceed 70 nm; so the sample can be considered as an assembly of single domain particles (in an ideal monodispersed system, with unique particle size, a single magnetic domain should be expected for manganite particles smaller than a critical size of 70 nm [23,24]).

The temperature dependences of resistivity and MR for fields up to 1.5 T of samples (not presented here) show the behavior characteristics of a conductive MTPS, similar to all appropriately doped (RE, A)MnO_3 compounds: exhibiting an insulating high-temperature paramagnetic phase, a metallic low-temperature ferromagnetic phase, a maximum near T_C and a negative CMR in a relatively small temperature range around T_C. The effect of Mn

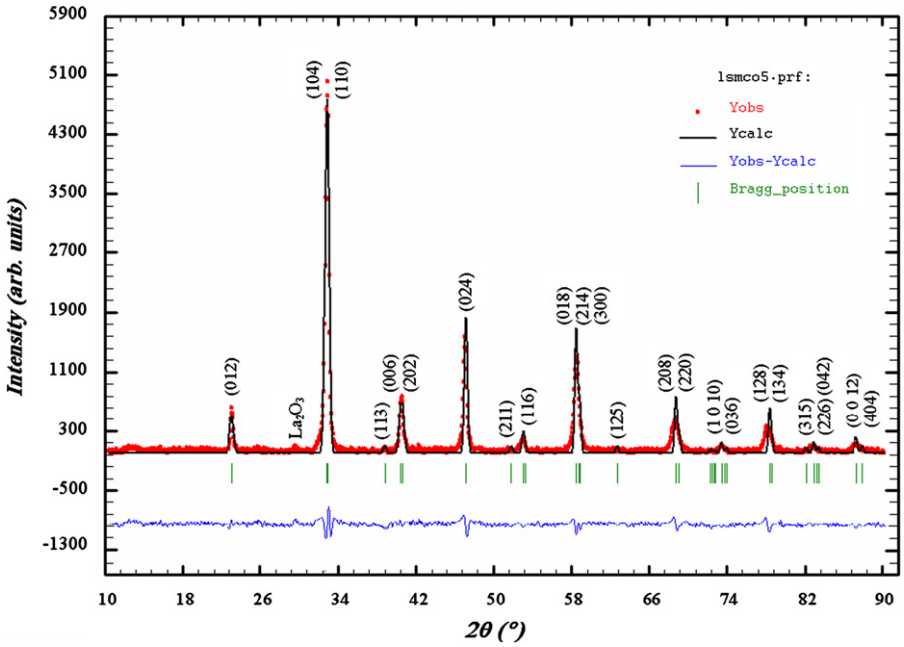

Fig. 1. The observed XRD pattern (the dots) and Reitveld-based calculated profile (the solid line) of nanoparticles of $LSMC_{0.05}O$ sample at room temperature. Tick marks below the profile indicate the positions of the allowed Bragg reflections. The difference curve (observed minus calculated) is plotted at the bottom (∗ indicates the peak due to La_2O_3 phase).

Table 1
Rhombohedral-cell lattice parameters of the $LSMC_xO$ compounds at room temperature.

Composition (x)	a (Å)	c (Å)	v (Å^3)
0	5.5076	13.4276	352.739
0.05	5.5065	13.3218	349.826
0.1	5.4841	13.3471	347.637

Table 2
Ionic radii of Co and Mn ions at different valence and spin states (HS and LS denote high and low spin states, respectively) [15].

Cation	Spin state	Ionic radius (Å)
Mn^{3+}	LS	0.58
	HS	0.65
Mn^{4+}	HS	0.53
Co^{3+}	LS	0.55
	HS	0.61
Co^{4+}	HS	0.53

substitution by Co is found to be a reduction in the metallic-insulator transition temperature of T_{MI}, and enhancement of resistivity and room temperature MR. This can be explained as follows: due to the small size of Co ions, their substitution results in reduction of volume and increase of Jahn–Teller distortion in the perovskite cell. This can lead to either a reduction in the Mn–O–Mn bond angle or a change in the bond length, both directly weakening the electron transfer and so the double-exchange mechanism, as discussed in [15–17,19,20]. The electrical resistivity and magnetoresistance at room temperature and the metal-insulator transition temperature (T_{MI}) of our $LSMC_xO$ samples are summarized in Table 3. As a comparison, the reported data for the samples with composition similar to the title compounds synthesized by the traditional solid state method are also presented [19]. Despite the general similarity between

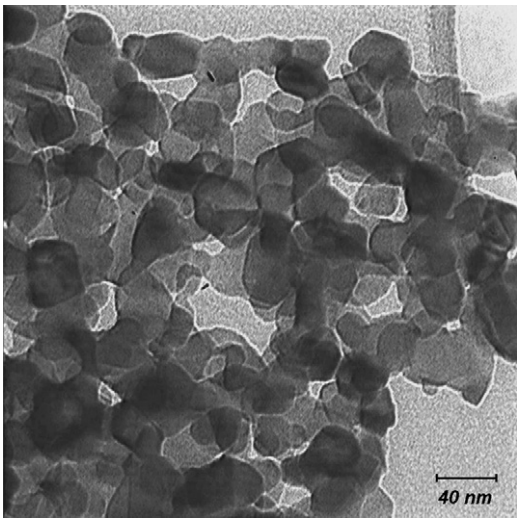

Fig. 2. A bright-field transmission electron image of the $LSMC_{0.1}O$ sample.

Table 3
Electrical resistivity (ρ_{RT}) and magnetoresistance ($MR|_{RT}$) at room temperature, and metal-insulator transition temperature (T_{MI}) of our $LSMC_xO$ samples compared with the reported values for similar compounds synthesized by traditional solid-state method.

Composition (x)	T_{MI} (K)	$\rho_{RT}\|_{H=0}$ (Ω cm)	$MR\|_{RT}$ ($H\sim1.5$ T) (%)
This work			
0	–	–	–
0.05	244	0.38	5
0.1	221	0.47	7
[16,19]:			
0.05	316	0.11	3
0.1	266	0.24	2

the electrical and magnetotransport behaviors of our samples and those in the literature, they have, as can be seen, a much lower T_{MI} and relatively larger values of ρ and MR, with respect to others.

This should be attributed to the nanometric size of particles, and this has been also observed in the case of other nanomanganite systems, such as $La_{0.7}Ba_{0.3}MnO_3$ [23] and $La_{0.7}Ca_{0.3}MnO_3$ [25,26]. The total resistivity ρ is assumed to be the sum of the bulk grain resistivity and the intergrain boundaries resistivity, and as the latter is much larger [26], our polycrystalline samples with their nanometric particle size have higher ρ values. Furthermore, since the maximum grain boundary resistivity occurs well below T_C [26], the decreased particle size can account for the lower observed T_{MI} values in our samples. The enhanced observed MR values can also be due to the nanometric grain size in our samples, since in granular manganites in addition to the intrinsic CMR, an extra kind of MR exists, IMR (absent in single crystals), due to spin-polarized tunneling between neighboring grains [27,28].

Fig. 3a shows the temperature dependence of linear thermal expansion $\Delta l/l$ of $LSMC_xO$ samples. It is well known that this dependence is almost linear for dia- and paramagnetic materials, due to the anharmonic phonon contribution, and is governed by the Grüneisen law. One can see that for each sample, an extra contribution over the usual anharmonic phonon contribution appears in a temperature range: beginning from T_C, the thermal expansion (TE) increases with temperature faster than the theoretical prediction. This anomalous behavior, observed similarly in ceramic samples of $la_{2/3}Ca_{1/3}MnO_3$ [4,5,10] and $La_{0.7}Ba_{0.3}MnO_3$ [9], is attributed to the gradual charge localization and local distortion originating from the formation of polarons (short-range FM clusters) at $T > T_C$. (The possibility of the presence of MTPS has been confirmed experimentally in the $La_{0.9}Sr_{0.1}MnO_3$ system [13].) As the lattice parameters are small in the FM parts [29], we have an extra contribution to the TE for $T > T_C$ due to the formation of ferro/antiferro-MTPS. Then, at a

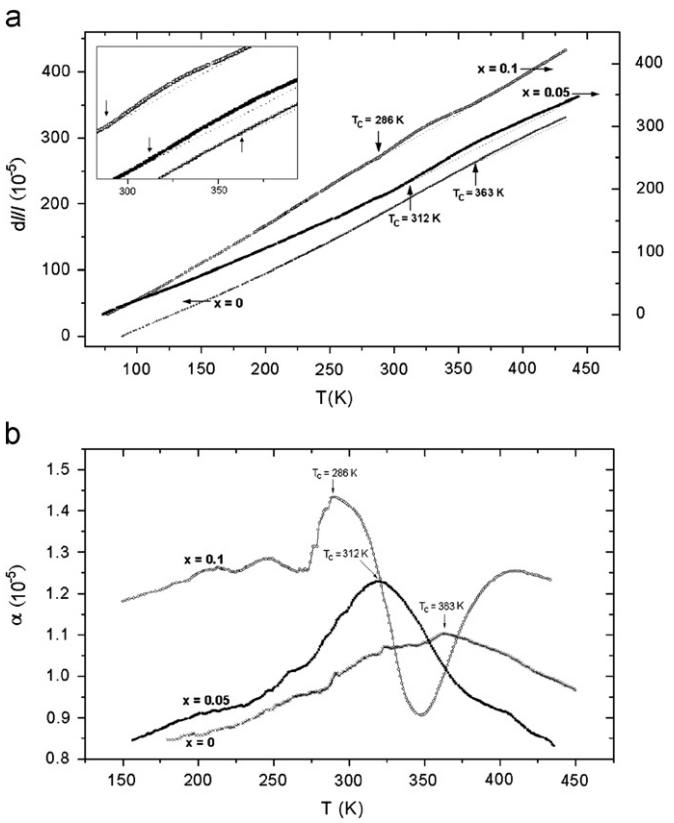

Fig. 3. (a) Temperature dependence of the linear thermal expansion of $LSMC_xO$ samples. The dashed lines show the simulated phonon contribution. (b) Thermal expansion coefficient vs. temperature for $LSMC_xO$ samples.

Table 4
Metal-insulator (T_{MI}) and parra-ferromagnetic transition temperatures of $LSMC_xO$ samples deduced from the anomalous behavior of TE (Fig. 3) and volume MS (Fig. 6), $T_{C,TE}$ and $T_{C,MS}$, respectively.

Composition (x)	T_{MI} (K)	$T_{C,TE}$ (K)	$T_{C,MS}$ (K)
0	–	363	364
0.05	244	312	296
0.1	221	286	278

higher temperature, this extra contribution vanishes by distortion of MTPS. Fig. 3b represents the temperature dependences of the thermal expansion coefficient α of the samples, which were determined by taking a point-to-point temperature derivative of the data in Fig. 3a. As can be seen, for all samples, α has a peak at T_C, and the slope change is well defined and continuous, indicating a second order PM–FM phase transition (no first order structural transition occurring). The T_C values of the samples estimated from the α curves are summarized in Table 4. The effect of Co substitution is the increase in α and reduction of T_C, attributed to the ionic size changes occurring because of changes in the spin states of Co ions at higher temperatures. It has been reported that as the temperature increases, the Co^{3+} ions undergo a transition from the low spin state with small diameter to the intermediate or high spin state with large size [20]. Therefore, increasing the Co content increases the amount of low spin to high spin transition and consequently, causes an enhancement in the α value. The reduction of T_C with Co substitution, which is also observed in other substitutions of (RE, A)MnO_3 at the Mn sites [17], can be due to double-exchange (DE) interaction weakening, resulting in the suppression of FM order.

The longitudinal ($\lambda_\parallel$), transverse ($\lambda_\perp$), anisotropic (λ_t) and volume magnetostriction (ω) isotherms of $LSMC_xO$ samples as a function of applied magnetic field at a selected temperature of 80 K are presented in Fig. 4. Since $\lambda_\parallel$ and $\lambda_\perp$ have opposite signs and large values, a large anisotropic magnetostriction (λ_t) is obtained. As can be seen, λ_t increases strongly in low fields and then tends towards saturation for all compounds. The observed abrupt change of λ_t in low-field region can be attributed to the conventional magnetostriction relevant to the domain-wall motion in the FM phase. In addition, it is clear from Fig. 4 that the saturation behavior of the MS occurs at different applied threshold fields for the studied samples. The threshold field increases by Co substitution. The temperature dependence of λ_t of the studied $LSMC_xO$ samples under the maximum magnetic field of 1.5 T is shown in Fig. 5. Since there are not any hysteric behaviors in these curves, it can be concluded that no field-induced structural phase transition takes place in these compounds in the studied temperature range. The behavior under lower fields is of the same manner. As can be seen, the anisotropic magnetostriction of all samples in the ferromagnetic phase ($T < T_C$) is relatively large ($\lambda_t \sim 10^{-4}$ at low temperatures) and then λ_t drops continuously to zero in the T_C region. This, qualitatively and quantitatively, is typical of anisotropic magnetostriction of a FM compound. From the observed λ_t behaviors of different compounds, one finds that Co substitution, in addition to lowering DE interaction, which in turn causes a reduction in T_C values, increases the magnetic anisotropy (λ_t increases about one order of magnitude with 10% Co substitution). This conclusion is consistent with the behavior of magnetization curves at low applied fields for these compounds [17]. Such a large anisotropic MS originates not only from the usual spin–orbit coupling mechanism but also probably from the orbital instability of the Co^{3+} ions under the magnetic field, giving rise to a transition from a low spin state ($S=0$) to an intermediate one ($S=1$) [30,31].

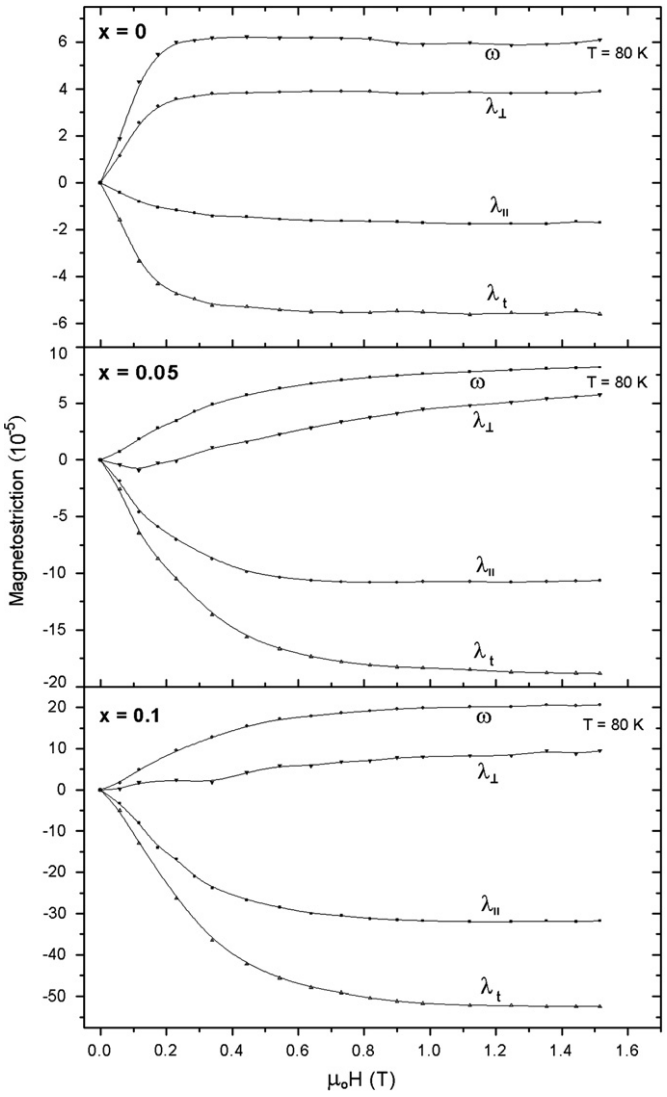

Fig. 4. Magnetostriction isotherms of $LSMC_xO$ samples vs. applied magnetic field at a selected temperature of 80 K.

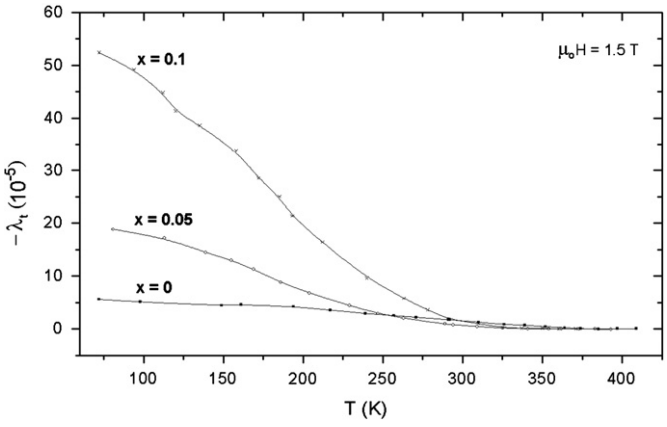

Fig. 5. Temperature dependence of anisotropic MS of $LSMC_xO$ samples at the maximum magnetic field of 1.5 T.

The temperature dependence of volume MS (ω) under magnetic field of 1.5 T is presented in Fig. 6 (the behavior under lower fields is the same). The behavior of ω in all samples has an abrupt change: it becomes negative and passes through an extremum value in the T_C region, and then with further temperature increase, it approaches zero. This unusual behavior (sample shrinkage under an applied field), which has been also observed in yttrium doped LCMO [4], is related to polaron effects and indicates the presence of a conductive MTPS (insulating AFM microregions in FM matrix) at $T \geq T_C$, which is expected for our samples with a high level of Sr^{2+} doping (more than 17% [3]). As mentioned, this MTPS is thermally destroyed in the T_C region, resulting in an extra contribution to TE. Applying the magnetic field at $T \geq T_C$ leads to stronger increase of FM order in the vicinity of impurities, and consequently, reconstructs the MTPS. The small lattice parameters in FM portions lead to sample shrinkage. However, the above-mentioned MTPS reconstruction by applied magnetic field takes place only in a limited temperature interval around T_C, so we have lattice shrinkage resulting in the observed increased negative ω value in the T_C region. Therefore, magnetostriction effects have two causes below and above T_C. Below T_C, MS is anisotropic and typical of a 3d FM metal, mainly due to spin alignment of magnetic ions spins under the applied magnetic field. Above T_C, charge delocalization is responsible for the observed behavior. This is common in all manganite perovskites [30]. However, in contrast to the reported temperature dependence of ω for LCMO [10] and LSMO compounds [13], whose ω values are negligible at low temperatures (due to the Jahn–Teller effect, exchange interaction and change in the magnetic moments), ω values of our samples at low temperatures increase with Co substitution. This is because the total MS of these Co-doped samples comes not only from Mn ions (due to their anisotropic exchange interaction and crystalline electric field) but also from Co ions with high anisotropy energy and large MS [17,32].

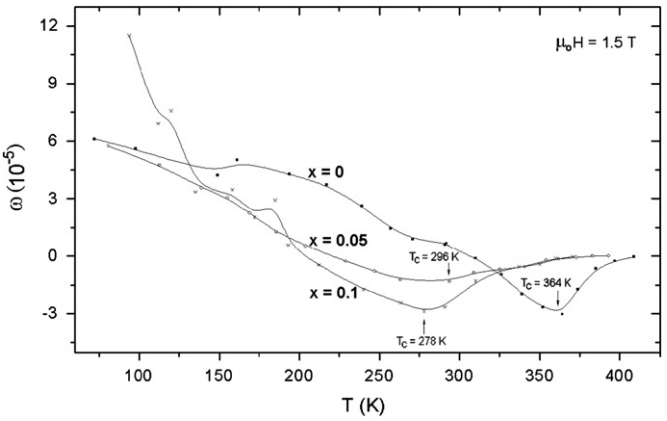

Fig. 6. Temperature dependence of volume MS of $LSMC_xO$ samples at the maximum magnetic field of 1.5 T.

The T_C values of samples estimated from the volume MS curves are also summarized in Table 4. The observed T_C (and T_{MI}) values are somehow smaller than the reported ones. This could be due to small particle size, resulting in the spin disorders near the surface of grains [27,33]. Furthermore, for each sample, the value of T_{MI} is lower than T_C, because at $T_{MI} < T < T_C$, there exist FM clusters in an insulating matrix, which grow under an applied magnetic field [14].

4. Conclusions

The effects of Co substitution on Mn sites in $La_{0.7}Sr_{0.3}MnO_3$ nanoparticles were studied and discussed in detail. In summary, Co substitution causes no structural transition and all compounds crystallize in rhombohedral symmetry with a space group of $R^{-}3c$.

However, due to the small ionic size of Co ions, a reduction in cell volume is observed. The Co substitution enhances the resistivity and magnetoresistance ratio and decreases the metal-insulator transition temperature T_{MI} that is attributed to the double-exchange interaction weakening. The anomalous behavior of magnetoresistance, volume magnetostriction and thermal expansion of these samples near T_C, like that of other manganites, can be explained based on a magnetic two-phase state. The thermal expansion coefficient, volume magnetostriction and anisotropic magnetostriction also increase with increase in Co content due to higher anisotropy energy of Co, its large magnetostriction effect and the change in Co ionic size occurring because of its spin state transitions at higher temperatures and under applied magnetic field. The relatively lower observed values for T_{MI} and $T_{C,}$ higher resistivity and MR, compared with the reported values for similar compounds with larger particle size, is attributed to the nanometric grain size and spin-polarized tunneling between neighboring grains.

Acknowledgement

The authors would like to thank Z. Kazemi for sample preparation and transport measurements. This work was supported by the Faculty of Sciences of Ferdowsi University of Mashhad under Grant No. 1374/p date 1.3.2009.

References

[1] A. Asamitsu, Y. Moritomo, R. Kumai, Y. Tomioka, Y. Tokura, Phys. Rev. B 54 (1996) (1716).
[2] A. Asamitsu, Y. Moritomo, Y. Tomioka, T. Arima, Y. Tokura, Nature 373 (1995) 407.
[3] L.I. Koroleva, R.V. Demin, A.V. Kozlov, D.M. Zashcherinskii, O.Yu. Gorbenko, A.R. Kaul, O.V. Melnikov, Ya.M. Mukovskii, J. Magn. Magn. Mater. 316 (2007) e644.
[4] M.R. Ibarra, P.A. Algarabel, C. Marquina, J. Blasco, J. García, Phys. Rev. Lett. 75 (1995) 3541.
[5] J.M. De Teresa, J. Blasco, M.R. Ibarra, J. García, C. Marquina, P. Algarabel, A. del Moral, J. Appl. Phys. 79 (1996) 5175.
[6] Jian Wu, Shi-Yuang Zhang, J. Magn. Magn. Mater. 264 (2003) 102.
[7] L.I. Koroleva, R.V. Demin, A.V. Kozlov, D.M. Zashchirinskiĭ, Ya.M. Mukovskiĭ, Zh. Éksp. Teor. Fiz. 131 (2007) 85;
[] L.I. Koroleva, R.V. Demin, A.V. Kozlov, D.M. Zashchirinskiĭ, Ya.M. Mukovskiĭ, JETP (Engl. Transl.) 104 (2007) 76.
[8] L.I. Koroleva, R.V. Demin, A.I. Abramovich, D.M. Zashcherinskii, A.V. Kozlov, V.Y.u Pavlov, Izv. RAN: Fiz. 71 (2007) 1623;
[] L.I. Koroleva, R.V. Demin, A.I. Abramovich, D.M. Zashcherinskii, A.V. Kozlov, V.Y.u Pavlov, BRAS: Phys. (Engl. Transl.) 71 (2007) 1581.
[9] R.V. demin, L.I. Koroleva, Ya.M. Mukovskii, J. Phys.: Condens. Matter 17 (2005) 221.
[10] J.M. De Teresa, M.R. Ibarra, J. Blasco, J. García, C. Marquina, P.A. Algarabel, Z. Arnold, K. Kamenev, C. Ritter, R. von Helmolt, Phys. Rev. B 54 (1996) 1187.
[11] J.J. Neumeier, K. Andres, K.J. McClellan, Phys. Rev. B 59 (1999) 1701.
[12] L.I. Koroleva, R.V. Demin, A.M. Balbashov, JETP Lett. 65 (1997) 474.
[13] R.V. demin, L.I. Koroleva, r. Szymszak, H. Szymszak, Pis'ma Zh. Éksp. Teor. Fiz. 75 (2002) 402;
[] R.V. demin, L.I. Koroleva, r. Szymszak, H. Szymszak, JETP Lett. (Engl. Transl.) 75 (2002) 331.
[14] X.K. Hu, M.H. Xu, Z.S. Wang, S.Y. Zhang, Q. Wu, P.Z. Si, Solid State Commun. 149 (2009) 243.
[15] J.B. Shi, F.C. Wu, C.T. Lin, Appl. Phys. A 68 (1999) 577.
[16] X.J. Fan, J.H. Zhang, X.G. Li, W.B. Wu, J.Y. Wang, T.J. Lee, H.C. Ku, J. Phys.: Condens. Matter 11 (1999) 3141.
[17] T.S. Zhao, W.X. Xianyu, B.H. Li, Z.N. Qian, J. Alloys Compd. 459 (2008) 29.
[18] M. Sugantha, R.S. Singh, A. Guha, A.K. Raychaudhuri, C.N.R. Rao, Mater. Res. Bull. 33 (1998) 1129.
[19] Jifan Hu, Hongwei Qin, Juan Chen, R.K. Zheng, J. Appl. Phys. 91 (2002) 8912.
[20] R.V. Wanderkar, B.N. Wani, S.R. Bharadwaj, Solid state Sci. 11 (2009) 240.
[21] Y. Ying, N.V. Dai, T.W. Eom, Y.P. Lee, J. Appl. Phys. 105 (2009) 093924.
[22] T. Zhu, C.H. Yan, Z.M. Wang, H.W. Zhao, J.R. Sun, B.G. Shen, Solid State Commun. 117 (2001) 471.
[23] S.K. Mandal, T.K. Nath, V.V. Rao, J. Phys.: Condens. Matter 20 (2008) 385203.
[24] D.G. Lamas, A. Caneiro, D. Niebieskikwiat, R.D. Sànchez, D. García, B. Alascio, J. Magn. Magn. Mater. 241 (2002) 207.
[25] J. Rivas, L.E. Hueso, A. Fondado, F. Rivadulla, M.A. López-Quintela, J. Magn. Magn. Mater. 221 (2000) 57.
[26] L.E. Hueso, F. Rivadulla, R.D. Sánchez, D. Caeiro, C. Jardón, C. Vázquez-Vázquez, J. Rivas, M.A. López-Quintela, J. Magn. Magn. Mater. 189 (1998) 321.
[27] M.A. López-Quintela, L.E. Hueso, J. Rivas, F. Rivadulla, Nanotechnology 14 (2003) 212.
[28] H.Y. Hwang, S.-W. Cheong, N.P. Ong, B. Batlogg, Phys. Rev. Lett. 77 (1996) 2041.
[29] A. Yanase, T. Kasuya, J. Phys. Soc. Jpn 25 (1968) 1025.
[30] H. Szymczak, J. Magn. Magn. Mater. 211 (2000) 186.
[31] H. Szymczak, R. Szymczak, Smart materials for ranging systems, in: J. Franse et al. (Ed.), NATO Science Series II, vol. 226, Springer, 2006, p. 245.
[32] M.R. Ibarra, R. Mahendiran, C. Marquina, B. García-Landa, J. Blasco, Phys. Rev. B 57 (1998) R3217.
[33] S. Das, P. Chowdhury, T.K. Gundu Rao, D. Das, D. Bahadur, Solid State Commun. 121 (2002) 691.